Hydrodynamics Defines the Stable Swimming Direction of Spherical Squirmers in a Nematic Liquid Crystal

Juho S Lintuvuori, Aloïs Würger, K. Stratford

Hydrodynamics Defines the Stable Swimming Direction of Spherical Squirmers in a Nematic Liquid Crystal

J. S. Lintuvuori,[1] A. Würger,[1] and K. Stratford[2]

[1]*Laboratoire Ondes et Matière d'Aquitaine, Université de Bordeaux & CNRS, 33405 Talence, France*
[2]*EPCC, University of Edinburgh, EH9 3FD, Edinburgh, United Kingdom*

We present a study of the hydrodynamics of an active particle a model squirmer in an environment with a broken rotational symmetry: a nematic liquid crystal. By combining simulations with analytic calculations, we show that the hydrodynamic coupling between the squirmer flow field and liquid crystalline director can lead to reorientation of the swimmers. The preferred orientation depends on the exact details of the squirmer flow field. In a steady state, pushers are shown to swim parallel with the nematic director while pullers swim perpendicular to the nematic director. This behavior arises solely from hydrodynamic coupling between the squirmer flow field and anisotropic viscosities of the host fluid. Our results suggest that an anisotropic swimming medium can be used to characterize and guide spherical microswimmers in the bulk.

Active materials use internal energy resources to propel themselves and have recently emerged as a topical research area within physics [1,2]. A natural example of an active system is provided by swimming bacteria, while artificial microswimmers can be realized by self-propelling Janus particles [3–10]. One big challenge is to control and direct the swimmers at the microscale. Success here could allow one to harness swimmers to do work, and it could lead to significant technological possibilities, for example, the direct microengineering of new materials.

Various possibilities have been explored in order to guide active particles. The most obvious one is to use confining walls, as both bacteria [11,12] and artificial swimmers [4,10,13–16] are known to be attracted to surfaces, and swim near them. Motion along predefined pathways can be obtained by topographical patterns [17] or chemical functionalization [18] of the surface. Force-free localization and steering of laser-powered Janus particles have been achieved by dynamical feedback [19] or by spatial modulation of the laser beam [20], which exerts a torque on the moving particle [21].

An alternative route to control the swimmers in the bulk is to use an anisotropic swimming medium [22], e.g., a liquid crystal [23]. Recent experiments with colloidal particles have demonstrated electrophoretic propulsion of spherical colloids in nematic liquid crystals (LCs) [23,24], whereas rodlike bacteria are observed to swim along the direction set by the nematic director $\hat{\mathbf{n}}$ [25–27]. Experimental applications include the self-assembly of bacteria dispersed in a nematic LC [28], transport of colloidal cargo [29], and the accumulation of the bacteria following topological patterns [30,31]. Theoretical predictions include anomalous diffusion [32] and even backward swimming was predicted by theoretical calculations of Taylor sheets in nematic LCs [33,34].

In the case of rodlike swimmers (e.g., typical bacteria) the alignment is dominated by an elastic energy, which is minimized when the rods align their long axis along $\hat{\mathbf{n}}$ [25]; thus, rodlike swimmers are always expected to swim following the nematic director. For isotropic swimmers (e.g., spherical bacteria or artificial Janus swimmers) this is not the case: in the limit of spherical particles the elastic torque vanishes.

In this Letter, we study the dynamics of fully resolved spherical microswimmers in a nematic liquid crystal, by means of lattice Boltzmann simulations and analytical calculations, using a squirmer model [35]. Our simulations show that the steady state swimming direction depends of the nature of the swimming mechanism. Spherical pushers undergo stable swimming following the direction set by the nematic director. Strikingly, a puller swims in steady state in a direction orthogonal to the far-field $\hat{\mathbf{n}}$. Using analytical calculations we show that the reorientation is due to a hydrodynamic torque, arising from the coupling between the squirmer flow field and anisotropy of the liquid crystalline viscosities [36]. Further, we show the reorientation rate scales linearly with the power of the squirmer flow field. Our results provide a robust and easy way to manipulate self-propelling organisms directly at the microscale, allowing, for example, the sorting of the swimmers based on their hydrodynamic nature.

Squirmer model.—To simulate the dynamics of an active particle in a liquid crystal we employ a lattice Boltzmann (LB) method [37]. We treat the self-propelling particle in the terms of a squirmer model [35]. The tangential (slip) velocity profile at the particle surface leading to the squirmer motions is given by [38]

$$u(\theta) = v_0 \sin(\theta)(1 + \beta \cos\theta), \quad (1)$$

where v_0 is a constant, β is the squirmer parameter, and θ is the polar angle with respect to the particle axis [13].

In the LB method a no-slip boundary condition at the fluid-solid interface can be achieved by using a standard method of bounce back on links [39,40]. When the boundary is moving (e.g., a colloidal particle) the bounce back on links condition needs to be modified to take into account particle motion [41]. These local rules can include additional terms, such as a surface slip velocity [Eq. (1)] leading to LB simulations of squirming motion [42,43].

Liquid crystal model.—The nematic host fluid is described by a Landau–de Gennes free energy whose density can be expressed in terms of a symmetric and traceless order parameter tensor $\mathbf{Q}$ as $\mathcal{F} = F(Q_{\alpha\beta}) + K/2(\partial_\beta Q_{\alpha\beta})^2$ with

$$F(Q_{\alpha\beta}) = A_0\left(1 - \frac{\gamma}{3}\right)\frac{Q_{\alpha\beta}^2}{2} - \frac{\gamma}{3}Q_{\alpha\beta}Q_{\beta\gamma}Q_{\gamma\alpha} + \frac{\gamma}{4}(Q_{\alpha\beta}^2)^2, \quad (2)$$

where the Greek indices denote Cartesian coordinates and summation over repeated indices is implied. A_0 is a free energy scale, γ is a temperaturelike control parameter giving an order-disorder transition at $\gamma \sim 2.7$, and K is an elastic constant. The anchoring at the particle surface is modeled by $f_s = W(Q_{\alpha\beta} - Q_{\alpha\beta}^0)^2$, where W is the anchoring strength and $Q_{\alpha\beta}^0$ is the preferred alignment of the nematic director at the particle surface.

The hydrodynamic equation for the evolution of $\mathbf{Q}$ is [44] $(\partial_t + u_\nu\partial_\nu)Q_{\alpha\beta} - S_{\alpha\beta} = \Gamma H_{\alpha\beta}$, where the first part describes the advection and $S_{\alpha\beta}$ describes the possible rotation or stretching of $\mathbf{Q}$ by the flow [44]. Γ is the rotational diffusion constant and the molecular field is

$$H_{\alpha\beta} = -\delta\mathcal{F}/\delta Q_{\alpha\beta} + (\delta_{\alpha\beta}/3)\mathrm{Tr}(\delta\mathcal{F}/\delta Q_{\alpha\beta}). \quad (3)$$

The fluid velocity obeys $\partial_\alpha u_\alpha = 0$ and the Navier-Stokes equation, which is coupled to the LC via a stress tensor. We employ a 3D lattice Boltzmann algorithm to solve the equations of motion (for further details see, e.g., Refs. [45,46]).

Simulation parameters.—We consider both pushers ($\beta < 0$) and pullers ($\beta > 0$). We fix $v_0 = 0.0015$, giving the particle velocity $u_0 \equiv \frac{2}{3}v_0 = 10^{-3}$ in lattice units, but vary the squirmer parameter in the range $\beta \in [-5, +5]$. We fix the fluid viscosity $\eta = 0.1$ and the swimmer radius $R = 4.0$ in lattice units [Fig. 1(a)]. To model the nematic liquid crystal we use $A_0 = 1.0$, $\gamma = 3.0$, $K = 0.01$, $\xi = 0.7$, $\Gamma = 0.3$, and a rotational viscosity $\gamma_1 = 2q^2/\Gamma = \frac{5}{3}$. The physics of our system is governed by the Reynolds (Re) and Ericksen (Er) numbers, which give the ratio of the inertial and viscous forces, as well as the ratio of the viscous and elastic force, respectively. Using the parameters above, we recover the following upper limits $\mathrm{Re} \equiv u_0 R/\eta \approx 0.04$ and $\mathrm{Er} \equiv \gamma_1 u_0 R/K \approx 0.68$. Simulations are carried out in a $64 \times 64 \times 64$ rectangular simulation box with periodic boundary conditions.

Results.—First, we consider the case where the particle surface does not impose an alignment of the nematic director ($W = 0$). We place a single swimmer into a nematic liquid crystal with an initial angle $\phi_0 = 45°$ between the squirmer orientation and $\hat{\mathbf{n}}$ [Fig. 1(a)]. For a puller ($\beta = +0.2$), the hydrodynamically induced torque rotates the particle away from the nematic director leading to a curved trajectory towards a direction perpendicular to $\hat{\mathbf{n}}$ [Figs. 1(b) and 1(c), solid lines]. A $\beta = -0.2$ pusher instead starts to turn in the opposite direction, leading to swimming in the direction set by the nematic director [Fig. 1(b), dashed line], reaching a steady state orientation $\phi \approx 0$ [Fig. 1(c), dashed line]. (See also Ref. [47] for additional movies of the puller and pusher).

The alignment of a pusher resembles the observation of bacterial swimmers in nematic LCs [25–29], which are known to be rodlike pushers. However, for rodlike swimmers there exists an elastic energy penalty of realignment that depends on the orientation ϕ with respect to $\hat{\mathbf{n}}$ and it is minimized when they align along $\hat{\mathbf{n}}$. The resulting elastic torque has been estimated as $T_{\mathrm{elastic}} \sim 4\pi K\phi L \ln(2L/R) \sim 10^5\phi$pNnm [25], which is considerably larger than that typically generated by the bacteria themselves $\sim 10^3$ pNnm [25,50]. Thus, rodlike swimmers are expected to always align along $\hat{\mathbf{n}}$ independently of their swimming mechanism. On the contrary, for spherical swimmers $T_{\mathrm{elastic}} = 0$; thus, any torque must arise solely from hydrodynamic interactions.

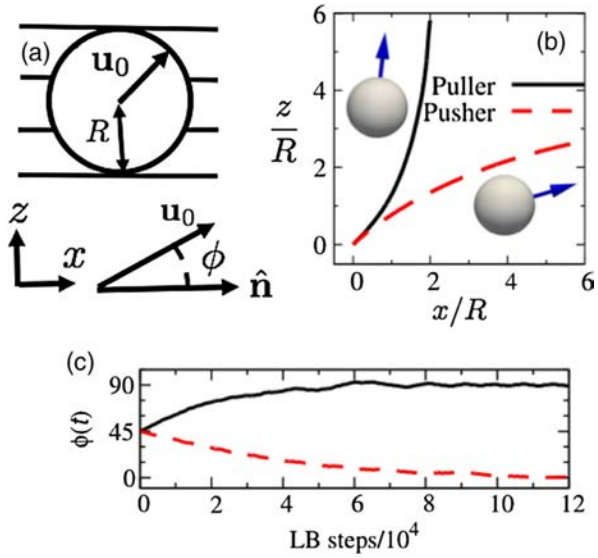

FIG. 1. (a) A cartoon showing the squirmer in a nematic liquid crystal, defining the angle ϕ used in the text, between the particle swimming direction $\mathbf{u}_0$ and the nematic director $\hat{\mathbf{n}}$. Examples of (b) the trajectory in the x z plane and (c) $\phi(t)$ observed in simulations of a puller ($\beta = +0.2$) and of a pusher ($\beta = -0.2$), with an initial orientation $\phi_0 = 45°$.

To analyze the underlying physical mechanism, we discuss how the squirmer's flow field $\mathbf{v}(\mathbf{r})$ interacts with a liquid crystal in terms of the nematohydrodynamic equations [47]. We study the torque exerted on the moving particle,

$$\mathbf{T} = \oint \mathbf{r} \times \sigma \cdot d\mathbf{S}, \tag{4}$$

where the integral runs over the particle surface having an oriented surface element $d\mathbf{S}$. A squirmer moving in an isotropic fluid with a viscosity $\eta_{\rm iso}$ has a flow field $\mathbf{v}_{\rm iso}(\mathbf{r})$. The viscous stress is defined as a linear function of velocity derivatives, $\boldsymbol{\sigma}_{\rm iso} = \eta_{\rm iso}\boldsymbol{\nabla}\mathbf{v}_{\rm iso}$, and for a spherical particle one has $\mathbf{T} = 0$. In a liquid crystal, the viscosity is an anisotropic fourth-rank tensor $\boldsymbol{\eta}$, and the stress is a rather intricate function of the strain $\boldsymbol{\nabla}\mathbf{v}$ and the order parameter $\mathbf{n}$. There is no analytical result for the squirmer velocity field $\mathbf{v}(\mathbf{r})$ in LCs [51]. We resort to a simple approximation that consists in evaluating the stress with the anisotropic viscosity $\boldsymbol{\eta}$ (given by the Leslie coefficients α_i for nematic LCs [47,52]) but using the velocity field $\mathbf{v}_{\rm iso}$ [53], in the limit of small Reynolds and Ericksen numbers.

From the velocity field of a moving squirmer $\mathbf{v}_{\rm iso}$, we readily obtain the stress and the nematohydrodynamic torque exerted on the particle (for a detailed calculation see the Supplemental Material [47]). The anisotropic part of the viscous stress is dominated by $\sigma - \sigma_{\rm iso} \propto \beta\boldsymbol{\eta}\hat{\mathbf{n}}(\hat{\mathbf{n}} \times \boldsymbol{\omega})$, where $\boldsymbol{\omega} = \boldsymbol{\nabla} \times \mathbf{v}_{\rm iso}$ is the vorticity of the flow field and $\boldsymbol{\eta}$ is the viscosity tensor. Inserting the known velocity field of a squirmer, we obtain the torque [47]

$$\mathbf{T}_N = -8\pi\beta\hat{\eta}v_0R^2(\hat{\mathbf{n}} \cdot \hat{\mathbf{u}})\hat{\mathbf{n}} \times \hat{\mathbf{u}}, \tag{5}$$

where $\hat{\mathbf{u}}$ is the particle axis. The effective viscosity coefficient $\hat{\eta} = \alpha_1/35 + (\alpha_2 + \alpha_3)/2 + (\alpha_5 + \alpha_6)/20$ is expressed in terms of the Leslie parameters α_i of a nematic liquid crystal [47] and is dominated by the coefficients $\alpha_{2,3}$ related to the rotational viscosities, while $\alpha_{1,5,6}$ corresponds to shear viscosities [47,52]. When $\beta\hat{\eta} > 0$, the torque aligns the particle axis on the order parameter. Throughout this Letter we assume $\hat{\eta} < 0$, which corresponds to measured values for common nematic LCs, e.g., pentylcyanobiphenyl (5CB) and *p*-methoxybenzylidene-*p*-butylaniline (MBBA), and to the simulations [47]. Then, Eq. (5) predicts that the stable orientation of pullers ($\beta > 0$) is perpendicular to the nematic order, whereas pushers ($\beta < 0$) move in the parallel direction. To test this predictions, we carried out simulations for a $\beta = +5$ puller and a $\beta = -5$ pusher, and initialized the system close to the unstable orientation. Figure 2(a) shows for the evolution of $\phi(t)$ an *S*-shaped trajectory, towards the stable positions given by Eq. (5).

To determine the angular velocity Ω, we match the torque T_N with the friction induced by the particle's rotation, $T_N - 8\pi\hat{\eta}_\Omega R^3\Omega = 0$, with the viscosity $\hat{\eta}_\Omega$ of the rotational Stokes drag [47]. Noting that the scalar and vector products in Eq. (5) result in a factor $\cos\phi \sin\phi = \frac{1}{2}\sin(2\phi)$, we find

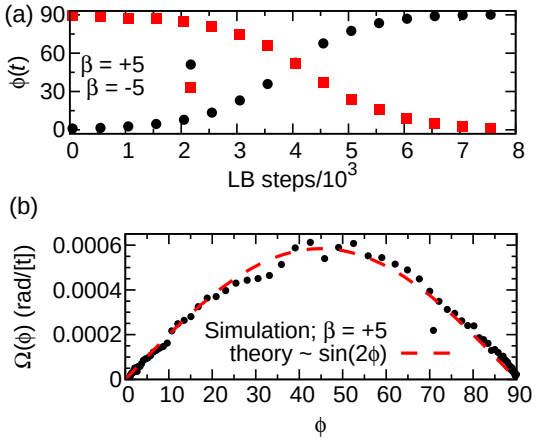

FIG. 2. (a) $\phi(t)$ exhibits an *S* shaped evolution, with a stable configuration $\phi \approx 90°$ ($\phi \approx 0°$) for a puller (pusher). (b) The rotational velocity $\Omega(\phi)$ is symmetric around $\phi = 45°$ and vanishes for $\phi \to 0$ and 90°, in agreement with theoretical arguments (see text for details).

$$\Omega = -\frac{1}{2}\beta \sin(2\phi)\frac{\hat{\eta}}{\hat{\eta}_\Omega}\frac{v_0}{R}. \tag{6}$$

The scale is given by v_0/R, and Ω is proportional to the squirmer parameter β and varies with the angle ϕ. In Fig. 2(b), this is compared with the numerical derivative $\Omega(\phi) = d\phi/dt$ from the simulation data for the $\beta = +5$ puller. The data show very good agreement between theory and numerics. Starting from the initial position $\phi = 0$, the simulated velocity increases linearly with ϕ, then reaches a maximum at $\phi \approx 45°$, and finally slows down when approaching the stable orientation $\phi = 90°$.

Modifying the squirmer parameter β keeps the swimming speed constant, but changes the power of the squirmer flow field [4]. This far we have established that the sign of β defines the stable swimming direction with respect to the nematic axis. To understand how the magnitude of the hydrodynamically induced torques depend on the power of the squirmer flow field, we initialize the simulations with $\phi_0 = 45°$, and systematically vary β between -5 and $+5$. We evaluate $\Omega(\beta)$ from a linear fit to early times on $\phi(t)$ data [see, e.g., early times in Fig. 1(c)]. $\Omega(\beta)$ from simulations shows a linear dependence for all the values of β considered (Fig. 3) and indeed the theory predicts $\Omega(\beta) \sim \beta$ for a fixed ϕ [see, e.g. Eq. (6)].

Interestingly, our numerical simulation results show that the reorientation dynamics for pullers is slightly more rapid than for pushers [see Fig. 1(c) and the inset in Fig. 3 for $\beta = \pm 0.2$). Also the angular velocity shown in Fig. 3 does not vanish at $\beta = 0$ (inset of Fig. 3) but in a steady state a neutral squirmer swims perpendicular to $\hat{\mathbf{n}}$ [see the Supplemental Material [47] for $\phi(t)$ for $\beta = 0$]. This behavior is not captured by our analytics. In our theoretical treatment we replace $\mathbf{v}(\mathbf{r})$ with the velocity field calculated in an isotropic liquid $\mathbf{v}_{\rm iso}(\mathbf{r})$. The analytical results agree

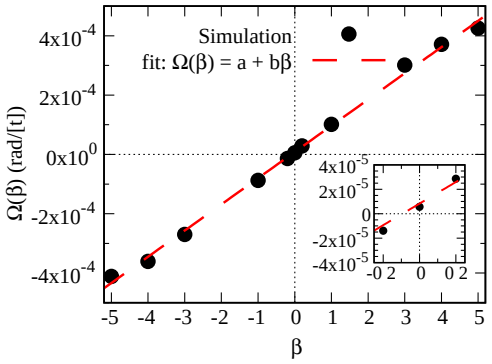

FIG. 3. The rotational velocity $\Omega(\beta)$ shows a linear dependence of the squirming parameter β for a fixed ϕ. For $\beta = 0$, Ω takes a value $a \approx 8 \times 10^{-6}[\mathrm{rad}/(t)]$ (see inset and text for details).

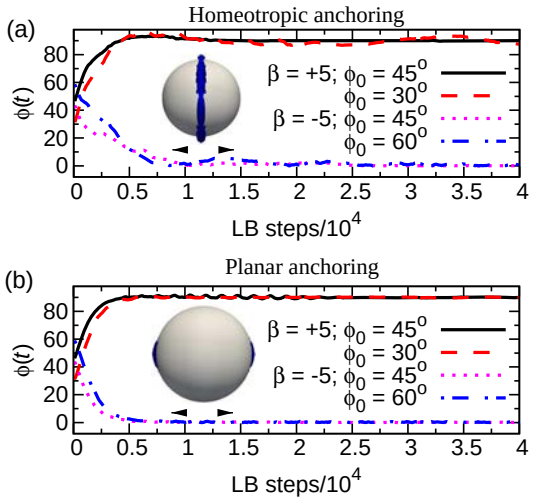

FIG. 4. The angle $\phi(t)$ for particles with (a) homeotropic and (b) planar anchoring of the nematic director at the particle surface ($WR/K \approx 4$) for both a puller ($\beta = +5$) and a pusher ($\beta = -5$). The insets show the defect structure around a passive particle: (a) Saturn ring defect for a homeotropic anchoring and (b) two boojums for a planar anchoring at the particle surface. (The arrow denotes the orientation of the far field nematic director).

remarkably well with the (more precise) numerical simulations, concerning the dependencies of Ω on the squirmer parameter β and the orientational angle ϕ [see, e.g., Fig. 2(b) and Fig. 3]. This is in line with a previous study of anisotropic diffusion of colloids, where this approximation was shown to compare favorably with numerically exact results [53]. The reorientation of a $\beta = 0$ swimmer could probably be reproduced when using the exact velocity field $\mathbf{v}(r)$, which depends itself on the viscosity anisotropy $\boldsymbol{\eta}$.

In all the examples above, we have considered a case where there is no anchoring at the nematic director at the surface of the colloidal particle ($W = 0$). Typically, in experiments the particle surface interacts with the nematic director ($W > 0$). The case of homeotropic anchoring can lead to the formation of a Saturn ring defect near the particle surface [see, e.g., the inset in Fig. 4(a)]. In the case of degenerate planar anchoring, two boojums are observed at both poles of the particle [inset of Fig. 4(b)]. We still observe the reorientation of the squirmers when a reasonably strong surface anchoring is included ($WR/K = 4$), as shown in Fig. 4 for a $\beta = +5$ puller and a $\beta = -5$ pusher. This provides further evidence that the reorientation is due to the hydrodynamic coupling between the squirmer flow field and the anisotropic viscosities of the LC, as opposed to short range elastic interactions.

Our main finding is that a nematic liquid crystal exerts a torque on a spherical microswimmer. This should be easily observable in experiments. Using typical values for the LC viscosities [47,52], and for microswimmers ($R \sim 1$ μm and $v_0 \sim 1$–10 μm/s), we can estimate the magnitude of the torque (5) $T \sim 4\beta \times (10^2$–$10^3)$ pN nm, and $\Omega \sim \beta(\mathrm{rad}/s)$, which is comparable to the recently observed rotation induced by a laser intensity gradient on a thermally powered Janus particle [20,21]. Further, the reorientation rate Ω is much faster than typical rotational diffusion. These, combined with the observation that the steady state behavior is retained for $WR/K > 0$, suggest that our prediction should be testable in the laboratory, for example, by dispersing artificial swimmers, e.g., Refs. [3–10,20] into standard nematic liquid crystals, e.g., 5CB or MBBA.

Conclusions.—We have presented a combined simulation and analytical calculation study of the steady state swimming of a spherical squirmer in a nematic liquid crystal. In a steady state a pusher will swim along the nematic director while a puller will be moving perpendicular to the direction set by the far-field $\hat{\mathbf{n}}$. We show via analytic calculations that the reorientation of the swimmers arises from the hydrodynamic coupling between the squirmer flow field and the anisotropicity of the liquid crystalline viscosities. For a passive spherical colloidal particle moving slowly in a thermotropic nematic LC a ratio of viscosities parallel ($||$) and perpendicular ($\perp$) to $\hat{\mathbf{n}}$ has been observed, $\eta_\perp/\eta_{||} \approx 2$, experimentally [54,55], and by both theoretical calculations and simulations [46,51]. Our calculations show that the anisotropy of the liquid crystal viscosities [36] gives rise to a hydrodynamic torque on the squirmer, leading to the observed steady state behavior. Finally, the steady state behavior persists even when a strong anchoring of the LC director at the particle surface is included, rendering it directly experimentally relevant. The predictions should be valid for spherical microswimmers.

A good candidate for an experimental realization of the predictions would be to consider a lyotropic nematic liquid crystal [53], for both artificial or bacterial swimmers. Here, recent experiments of a diffusion of colloidal particles showed a viscosity ratio $\eta_\perp/\eta_{||} \sim 4$ [53], which is a larger anisotropy than considered here. Using thermotropic (oil-based) LCs would require particles capable of swimming in oil. The predictions presented here could also be valid for a

wider class of materials that exhibit anisotropic viscosities, e.g., lyotropic lamellar phases could an interesting host material for future studies. Our results suggest that anisotropic materials could offer an exciting, yet easy-to-use, platform to guide microswimmers in the bulk. This could allow, for example, directed transport, or the sorting of swimmers based on their hydrodynamic signature, by simply dispersing them into an environment with a broken symmetry (e.g., a nematic liquid crystal).

J. S. L. acknowledges funding from IdEx (Initiative d'Excellence) Bordeaux Junior Chair. A. W. acknowledges support by the Agence Nationale de la Recherche through Contract No. ANR-13-IS04-0003.

[1] S. Ramaswamy, Annu. Rev. Condens. Matter Phys. **1**, 323 (2010).
[2] M. C. Marchetti, J. F. Joanny, S. Ramaswamy, T. B. Liverpool, J. Prost, M. Rao, and R. A. Simha, Rev. Mod. Phys. **85**, 1143 (2013).
[3] A. T. Brown and W. C. K. Poon, Soft Matter **10**, 4016 (2014).
[4] A. T. Brown, I. D. Vladescu, A. Dawson, T. Visser, J. Schwarz Linek, J. S. Lintuvuori, and W. C. K. Poon, Soft Matter **12**, 131 (2016).
[5] S. J. Ebbens, G. A. Buxton, A. Alexeev, A. Sadeghi, and J. R. Howse, Soft Matter **8**, 3077 (2012).
[6] B. Sabass and U. Seifert, Phys. Rev. Lett. **105**, 218103 (2010).
[7] S. Ebbens, M. H. Tu, J. R. Howse, and R. Golestanian, Phys. Rev. E **85**, 020401 (2012).
[8] S. Ebbens, D. Gregory, G. Dunderdale, J. Howse, Y. Ibrahim, T. Liverpool, and R. Golestanian, Europhys. Lett. **106**, 58003 (2014).
[9] X. Wang, M. In, C. Blanc, M. Nobili, and A. Stocco, Soft Matter **11**, 7376 (2015).
[10] S. Das, A. Garg, A. I. Campbell, J. Howse, A. Sen, D. Velegol, R. Golestanian, and S. J. Ebbens, Nat. Commun. **6**, 8999 (2015).
[11] Lord Rothschild, Nature (London) **198**, 1221 (1963).
[12] A. P. Berke, L. Turner, H. C. Berg, and E. Lauga, Phys. Rev. Lett. **101**, 038102 (2008).
[13] K. Ishimoto and E. A. Gaffney, Phys. Rev. E **88**, 062702 (2013).
[14] A. Zöttl and H. Stark, Phys. Rev. Lett. **112**, 118101 (2014).
[15] G. J. Li and A. M. Ardekani, Phys. Rev. E **90**, 013010 (2014).
[16] J. S. Lintuvuori, A. T. Brown, K. Stratford, and D. Marenduzzo, Soft Matter **12**, 7959 (2016).
[17] J. Simmchen, J. Katuri, W. E. Uspal, M. N. Popescu, M. Tasinkevych, and S. Sánchez, Nat. Commun. **7**, 10598 (2016).
[18] W. E. Uspal, M. N. Popescu, S. Dietrich, and M. Tasinkevych, Phys. Rev. Lett. **117**, 048002 (2016).
[19] A. Bregulla, H. Yang, and F. Cichos, ACS Nano **8**, 6542 (2014).
[20] C. Lozano, B. ten Hagen, H. Löwen, and C. Bechinger, Nat. Commun. **7**, 12828 (2016).
[21] T. Bickel, G. Zecua, and A. Würger, Phys. Rev. E **89**, 050303(R) (2014).
[22] A. E. Patteson, A. Gopinath, and P. E. Arratia, Curr. Opin. Colloid Interface Sci. **21**, 86 (2016).
[23] O. D. Lavrentovich, Curr. Opin. Colloid Interface Sci. **21**, 97 (2016).
[24] S. Hernàndez Navarro, P. Tierno, J. Ignés Mullol, and F. Sagués, Soft Matter **9**, 7999 (2013).
[25] I. I. Smalyukh, J. Butler, J. D. Shrout, M. R. Parsek, and G. C. L. Wong, Phys. Rev. E **78**, 030701 (2008).
[26] A. Kumar, T. Galstian, S. K. Pattanaeyk, and S. Rainville, Mol. Cryst. Liq. Cryst. **574**, 33 (2013).
[27] S. Zhou, A. Sokolov, O. D. Lavrentovich, and I. S. Aranson, Proc. Natl. Acad. Sci. U.S.A. **111**, 1265 (2014).
[28] P. C. Mushenheim, R. R. Trivedi, H. H. Tuson, D. B. Weibel, and N. L. Abbott, Soft Matter **10**, 88 (2014).
[29] R. R. Trivedi, R. Maeda, N. L. Abbott, S. E. Spagnolie, and D. B. Weibel, Soft Matter **11**, 8404 (2015).
[30] C. Peng, T. Turiv, Y Guo, Q. H. Wei, and O. D. Lavrentovich, Science **354**, 882 (2016).
[31] M. M. Genkin, A. Sokolov, O. D. Lavrentovich, and I. S. Aranson, Phys. Rev. X **7**, 011029 (2017).
[32] J. Toner, H. Löwen, and H. H. Wensink, Phys. Rev. E **93**, 062610 (2016).
[33] M. S. Krieger, S. E. Spagnolie, and T. Powers, Soft Matter **11**, 9115 (2015).
[34] M. S. Krieger, M. A. Dias, and T. Powers, Eur. Phys. J. E **38**, 94 (2015).
[35] M. J. Lighthill, Commun. Pure Appl. Math. **5**, 109 (1952).
[36] M. Miesovicz, Nature (London) **158**, 27 (1946).
[37] M. E. Cates, K. Stratford, R. Adhikari, P. Stansell, J. C. Desplat, I. Pagonabarraga, and A. J. Wagner, J. Phys. Condens. Matter **16**, S3903 (2004).
[38] V. Magar, T. Goto, and T. J. Pedley, Q. J. Mech. Appl. Math. **56**, 65 (2003).
[39] A. J. C. Ladd, J. Fluid Mech. **271**, 285 (1994).
[40] A. J. C. Ladd, J. Fluid Mech. **271**, 311 (1994).
[41] N. Q. Nguyen and A. J. C. Ladd, Phys. Rev. E **66**, 046708 (2002).
[42] I. Llopis and I. Pagonabarraga, J. Non Newtonian Fluid Mech. **165**, 946 (2010).
[43] I. Pagonabarraga and I. Llopis, Soft Matter **9**, 7174 (2013).
[44] A. N. Beris and B. J. Edwards, *Thermodynamics of Flowing Systems* (Oxford University Press, Oxford, 1994).
[45] J. S. Lintuvuori, K. Stratford, M. E. Cates, and D. Marenduzzo, Phys. Rev. Lett. **105**, 178302 (2010).
[46] J. S. Lintuvuori, K. Stratford, M. E. Cates, and D. Marenduzzo, J. Mater. Chem. **20**, 10547 (2010).
[47] See Supplemental Material at http://link.aps.org/supplemental/10.1103/PhysRevLett.119.068001, which includes Refs. [48,49], the supplementary Fig. S1, movies (M1 and M2), the calculation of the Leslie viscosities for the lattice Boltzmann model, and additional information on the nematohydrodynamic calculations.
[48] D. Marenduzzo, E. Orlandini, M. E. Cates, and J. M. Yeomans, Phys. Rev. E **76**, 031921 (2007).
[49] H. Stark, Phys. Rep. **351**, 387 (2001).

[50] N. C. Darnton, L. Turner, S. Rojevsky, and H. C. Berg, J. Bacteriol. **189**, 1756 (2007).
[51] H. Stark and D. Ventzki, Phys. Rev. E **64**, 031711 (2001).
[52] P. G. de Gennes and J. Prost, *The Physics of Liquid Crystals,*, 2nd ed. (Clarendon Press, Oxford, 1993).
[53] F. Mondiot, J. C. Loudet, O. Mondain Monval, P. Snabre, A. Vilquin, and A. Würger, Phys. Rev. E **86**, 010401(R) (2012).
[54] J. C. Loudet, P. Hanusse, and P. Poulin, Science **306**, 1525 (2004).
[55] H. Gleeson, T. A. Wood, and M. Dickinson, Phil. Trans. R. Soc. A **364**, 2789 (2006).